"Enhanced approach of assessing the corrosive wear of engineering materials under impingement"

L Giourntas[a], T Hodgkiess[b], A M Galloway[a]

[a]Department of Mechanical and Aerospace Engineering, University of Strathclyde, Glasgow

[b]Porthan Limited, Lochgilphead, Scotland

lampros.giourntas@strath.ac.uk

Abstract

Corrosive wear phenomena are apparent in hydraulic machinery that handle slurries. This study focuses on the development of an integrated methodology of material assessment that is employed to understand the mechanisms of deterioration and effectively compare materials' performance under impinging slurry. The technique involves mass loss measurements and post-test analysis of the surface, which comprises measurement of wear scar depths and volumes, that yield the quantification of the various material degradation processes that occur directly under, and adjacent to, the impinging jet. A medium carbon steel and a stainless steel have been investigated, since they exhibit different corrosive wear behaviour.

Key words

Corrosive wear, Sliding Abrasion, Steels, Jet impingement

1. Introduction

In a wide range of industrial situations, problems arise when a stream of water impinges on, or flows over, components. The consequent deterioration process is, of course, exacerbated when the aqueous fluid is severely corrosive and also when it contains suspended particles that may range in size from fine sand through to large mineral particles. Methods of combating the erosion-corrosion phenomena, understandably, have attracted a substantial interest in the research community where relevant factors associated both with the environmental parameters and materials/coatings performance has been intensively investigated.

A number of experimental techniques have been adopted for study of these types of corrosive wear of which the most common appears to be the submerged jet apparatus [1,2], but other important methods are slurry pot [3], Coriolis [4,5] and rotating cylinder [6]. Approaches that involve mapping of the inter-relationship between erosion corrosion damage and environmental parameters, have also been utilised [7,8]. Another desirable approach involves mathematical modelling of corrosive wear which often makes use of CFD packages to predict flow regimes [9][10]. Although there have been some interesting studies, for instance focusing on modelling damage immediately under a perpendicularly-impinging slurry [11], there are formidable obstacles to this type of approach when dealing with such a complex phenomenon. Thus, at present at least, it is evident that the main thrust of research into corrosive wear must depend on experimental investigations.

The focus of the present paper is the most widely-used experimental technique; submerged jet. In such experiments, an aqueous stream, with or without solid particles, is directed onto a specimen whose surface area is greater than the diameter of the jet. The great majority of test programmes have adopted a 90° angle of impingement – although, of course, industrial equipment is subject to a range of angles[12].

Some studies have investigated the effect of angle of impingement in pure erosion conditions [13–15], where the classical theories [16] of the mechanical damage mechanisms are relevant. Other researchers have assessed also the erosion-corrosion behaviour over a range of impingement angles [1,17].

A basic feature of all jet impingement tests is that they involve a measurement of the specimen mass loss and such information has proved valuable in comparative exercises that compare different materials or test conditions. It must be recognised, however, that the total mass loss of a specimen, which is subjected to a typical submerged jet, is a measure of damage in two distinct regions;

- The directly impinged zone in which a distinct wear scar is produced
- The surrounding area over which the fluid is flowing at essentially zero (glancing) angle with an essentially abrasive action.

Whilst it is well-known that the localized damage is more severe in the directly impinged zone, the material loss is unlikely to be negligible in the area outwith the wear scar. Moreover, a change in component material or impinging fluid characteristics might result in differing relative magnitudes of damage in those two regions.

It is therefore apparent that the output from investigations that employ the submerged jet technique would be enhanced by post-test evaluation that included unravelling of the total mass loss into the two separate components of damage. This strategy will contribute to a deeper interpretation of fundamental mechanisms of corrosive wear and expanded data for industrial use. This is a tactic that, to the authors' knowledge, does not appear to have been employed hitherto. The key inspection method that will contribute to this objective is surface profiling/topography. There are several ways of undertaking topographical investigations; Atomic force microscopy (AFM), Interferometry, Stylus, and optical profiling. The simplest type of profiling is the line scan across a specimen surface which yields wear scar depths. Only a few research papers quote such measurements and, in any case, this approach does not directly provide the most desired information [4,11,18]. One such study did briefly involve an estimation of wear scar volume by employing solid geometry to measure values of wear scar depth and diameter on commercially-pure titanium alloy specimen after erosion corrosion [19]. Clearly, the optimum way of obtaining the wear scar volume is from 3-D surface profiling. Occasionally papers show such a 3-D image of a specimen after testing but do not quote any volumes resulting from the image [20]. One piece of work did measure the wear scar volumes of API X42 which had been subjected to dry sand erosion [14]. Other researchers appear to have addressed the issue of comparing mass losses within the wear scar with the overall mass loss but within the focused context of corrosion inhibitor performance with limited data being presented [21].

The objective of the work described in the present paper was to extend the conventional scope of jet impingement test evaluation in order to obtain the additional information that is discussed above. To broaden this assessment, experiments were conducted on two steel alloys (a carbon steel and a stainless steel) that would be expected to behave rather differently in erosion corrosion conditions in solid/liquid impingement.

2. Methodology

The steels that were selected for this study are listed below:

- Austenitic stainless steel (UNS S31600), which exhibits good corrosion resistance in various corrosive environments.
- A medium carbon steel (UNS G10400), which has poor corrosion performance in most aqueous conditions.

Their typical compositions, as well as their hardness measured, on a Vicker's hardness machine with 5kgf, are shown on Table 1.

Material	C%	Cr%	Ni%	Mo%	S%	Mn%	Si%	N%	P%	Hardness (HV)
UNS S31600	≤0.08	16-18	10-14	2.0-3.0	≤0.03	≤2.0	≤0.75	≤0.1	0.045	200
UNS G10400	0.37-0.44				≤0.05	0.6-0.9			≤0.04	240

Table 1 Typical composition of the steels.

Mass loss measurements were carried out under solid/liquid impingement in both free erosion-corrosion conditions and also with the application of cathodic protection (CP) to clarify the mass loss due to mechanical deterioration mechanisms. Also, post-experimental analysis was facilitated with Alicona Infinite Focus equipment from which wear scar depths as well as volume losses were determined.

The erosion-corrosion experiments were carried out using a circulating closed loop rig (Figure 1). The duration of the tests was 1 hour. The nozzle diameter was 3 mm and the slurry, which consisted of 3.5% NaCl and sand particles, impinged at 19 m/s velocity perpendicular to the specimen surface. The silica sand particles used in this study possess hardness of 1160HV with spherical shape, as shown in Figure 2. The sand concentration, which was measured directly under the nozzle, was 150 mg/l. Table 2 represents the sand particle size distribution. The testing temperature range was 30^{o}C -36^{o}C. The specimens, of 38mm diameter, were ground on 220, 500, 800, and 1200 SiC grit papers. The distance between the specimens and the nozzle was fixed at 5mm. A mass balance of accuracy 0.1mg was used for the mass loss measurements. After the experiments, the medium carbon steel specimens were immersed briefly in an inhibited acid solution (Clark solution) before weighing due to the extensive corrosion on its surface. For the experiments that employed CP, the electrode potential was kept at -0.85mV (Ag/AgCl reference electrode) to suppress any electrochemical processes on the specimen. The surface topography was assessed on cathodically protected specimens in the same way as after free erosion-corrosion.

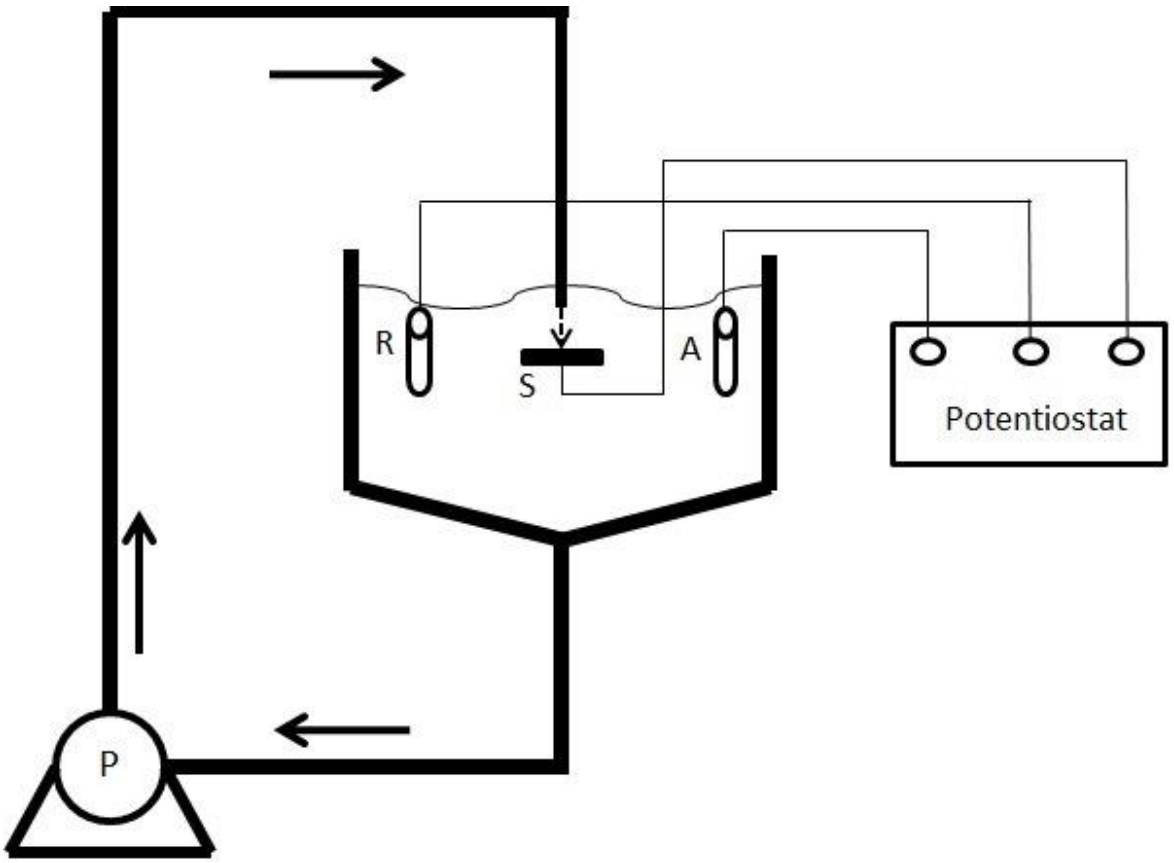

Figure 1. Schematic diagram of solid/liquid jet impingement circulating rig showing electrochemical equipment (A-Auxiliary Electrode, R-Reference Electrode, S- Specimen (Working Electrode))

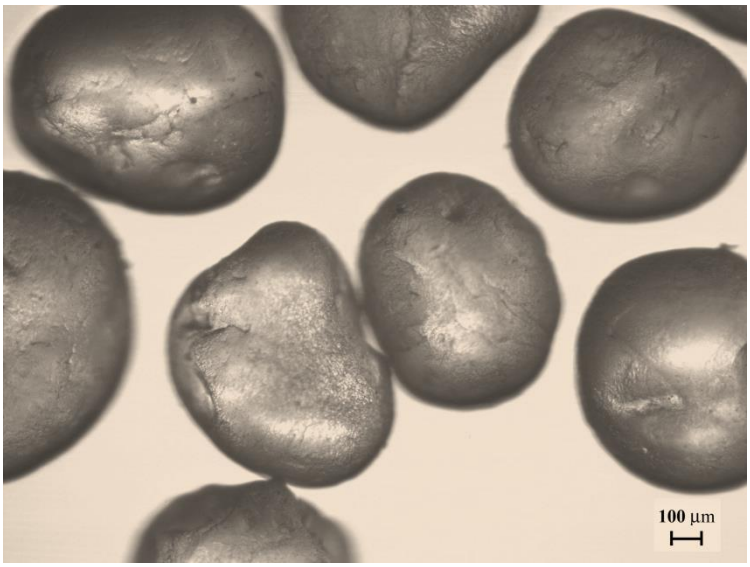

Figure 2. Microscopic view of the spherical shape silica sand.

Size (µm)	<250	251-355	356-420	421-500	501-600	601-710	>711
Mass (%)	0.05	3.2	5.3	18.3	70	3.1	0.05

Table 2. Size distribution of the silica sand used in solid/liquid impingement.

3. Results

3.1 Mass loss measurements

Figure 3 demonstrates the mass loss measurements as averages with error bars showing the scatter from the three replicates under free erosion-corrosion and also with the application of cathodic protection. The erosion-corrosion performance of the UNS S31600 was superior compared with the carbon steel UNS G10400. The discrimination of these two steels was evident in both conditions as the UNS S31600 sustained its superior resistance even when the cathodic protection was applied. It is also apparent that the UNS G10400 suffers severely by the corrosion factor, as its mass loss with the CP applied is almost half when no electrochemical processes are taking place (CP).

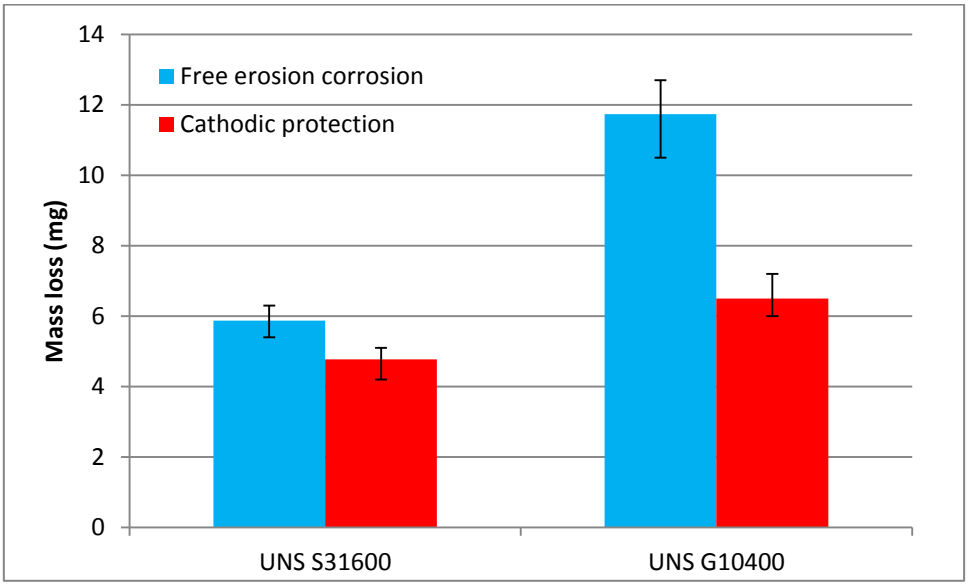

Figure 3. Mass loss of the steels in solid/liquid impingement with and without cathodic protection application

3.2 Surface Profile scans

To evaluate, more extensively, the behaviour of these two different metals in the zone directly under the impinging jet (wear scar), surface profile scans were completed on all specimens. Figures 4 and 5 show examples of U-shaped wear scar profiles of the stainless steel and the carbon steel respectively, after test in free erosion-corrosion conditions. It should be mentioned that the wear scar diameter corresponds approximately to the diameter of the nozzle.

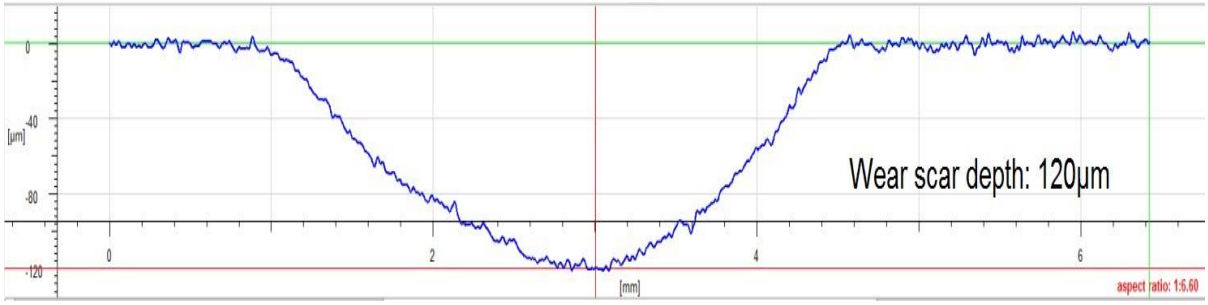

Figure 4. Surface profile scan of the wear scar of the stainless steel UNS S31600 after solid/liquid impingement.

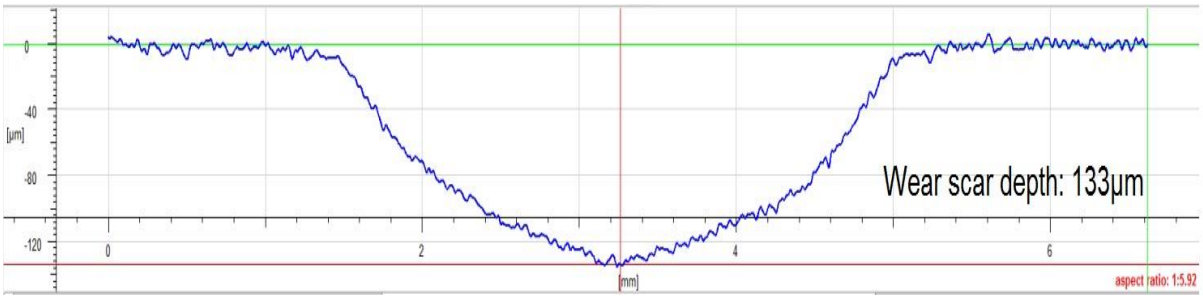

Figure 5. Surface profile scan of the wear scar of the medium carbon steel UNS G10400 after solid/liquid impingement.

Figure 6 shows the wear scar depths of the two steels with and without cathodic protection. There is a clear correlation between the mass losses and the wear scar depths, as the UNS G10400 has deeper wear scars than the UNS S31600. It is also evident, that the application of CP has not generally resulted in significant reduction in wear scar depth on either material.

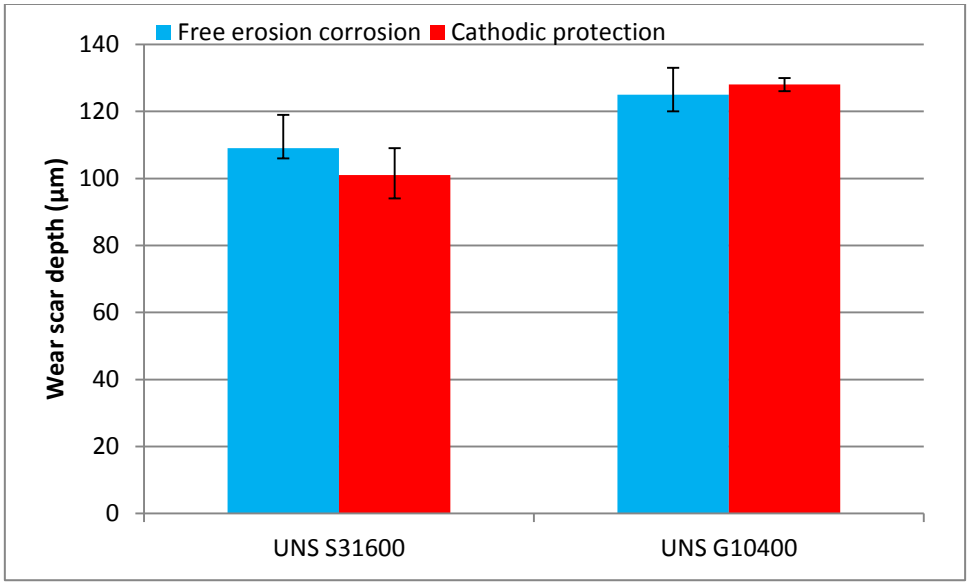

Figure 6. Wear scar depths of the studied materials in erosion corrosion conditions with and without cathodic protection.

3.3 Volumetric Analysis

Figure 7 shows the volume measurement of the direct impinged zone of the UNS S31600. The volumetric analysis was executed on the region inside the blue ring, which represents the area under the jet. It is clear, from the surface profile scan below, that the volume loss has been determined accurately within the wear scar. Also, several volume assessments have been undertaken by increasing the diameter of the blue ring and the differences in the resulting volume values were minimal. Possible inaccuracies/errors in the measured wear scar volume due to general thickness loss of the specimen surface during the 1hour experiment were calculated to be negligible.

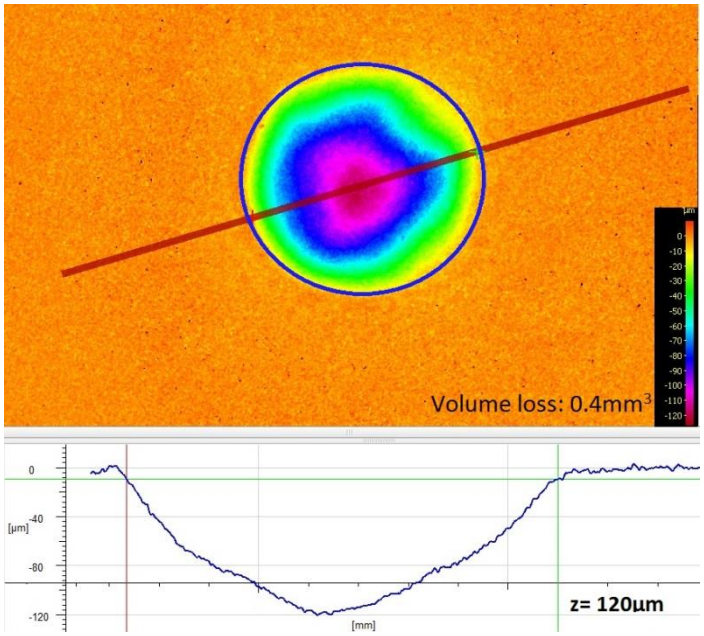

Figure 7. Volumetric analysis and surface scan on the direct impinged zone of the UNS S31600 surface after solid/liquid impingement without CP.

Figure 8 illustrates the volume losses within the wear scar during solid/liquid impingement with and without cathodic protection. The volume loss of the UNS G10400 steel was 20% higher than UNS S31600 in both conditions, which shows the benefit of the stainless steel over the medium carbon steel within the direct impinged zone. It is also evident that the volume losses remain stable, even if the cathodic protection current is applied to the specimens. This trend demonstrates that the volume loss on the direct impingement is mostly associated with erosion damage.

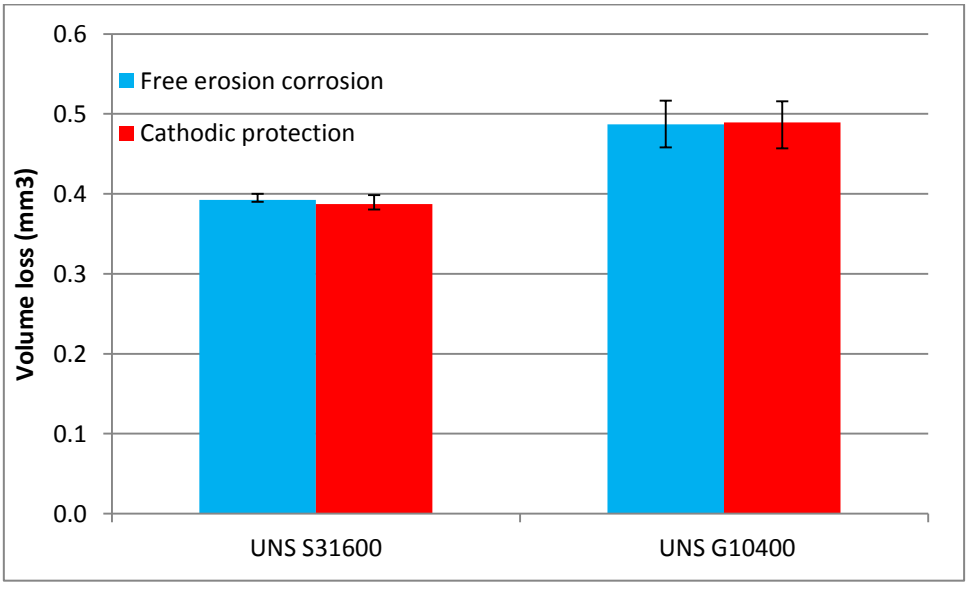

Figure 8. Comparison of the average volume losses within the wear scar of the UNS S31600 and UNS G10400 with and without cathodic protection.

4. Discussion

A comparison of the relative magnitudes of the various deterioration mechanisms taking place on both materials is represented in Figure 9. The separation of the various mechanisms is based on the recognized contributors to corrosive wear damage;

$$T = M + C + S \qquad \text{Equation 1}$$

Where T is the total mass loss, M is the mechanical damage, C is the pure electrochemical damage and S is the synergy of the electrochemical with the mechanical damage.

The values of Figure 9 have been obtained as described in the sections below.

Total Mass loss (TML) in free erosion corrosion (FEC) conditions

The total mass losses were measured directly, see Figure 3. The overall mass loss of the UNS S31600 was substantially lower than the UNS G10400 in free erosion corrosion conditions, which demonstrates the superiority of the stainless steels against carbon steels. This feature is mostly related with the nature of the stainless steels, which are well known corrosion resistant alloys (CRA's), and they form a passive film that protects them from corrosion.

The total mass loss is identified as the mass loss of the wear scar and the material loss beyond the direct impinged zone. In other words, it represents the erosion-corrosion phenomena, which appears within the wear scar, and the sliding abrasion/corrosion on the outer area. This identification of the degradation processes are displayed clearly in Equations 2 and 3 below:

$$TML\ (FEC) = ML\ [DIZ] + ML\ [OA] \qquad \text{Equation 2}$$

where TML (FEC) is the total mass loss at free erosion-corrosion conditions, ML[DIZ] is the mass loss on the direct impinged zone (DIZ) which is calculated from the measured volume losses and the material densities, and ML [OA], calculated in Table 3, represents the mass loss on the outer area (OA).

Table 3 demonstrates clearly that, for the UNS S31600 steel, the most substantive manifestation of damage caused by the submerged jet is the wear scar in the directly impinged zone. For the carbon steel however, corrosive wear damage in the outer area is much more significant and this feature precludes simple correlation of material loss with target hardness.

Materials	TML	ML [DIZ]	ML [OA]
UNS S31600	5.9 mg	($0.4mm^3$ x 8.0 g/cm^3) = 3.2 mg	2.7 mg
UNS G10400	11.7 mg	($0.49mm^3$ x 7.85 g/cm^3) = 3.9 mg	7.8 mg

Table 3. Breakdown of the total mass loss to the mass losses of the two regions for free erosion-corrosion

Consequently, separation of the mass losses in the two zones is clearly relevant to understanding the fundamental mechanisms of deterioration of components subjected to a submerged jet. It also facilitates comparisons of materials/coatings behaviour under two distinct corrosive wear situations. In addition to the overall subdivision of damage between two zones, it is possible to compute the magnitudes of damage due to the various components of corrosive wear.

$$TML\ (FEC) = E\ [DIZ] + (C+S)\ [DIZ] + SA\ [OA] + (C+S)\ [OA] \qquad \text{Equation 3}$$

Where, E [DIZ] is the erosion damage inside the wear scar, (C+S) [DIZ] is the corrosion related component on the wear scar, SA [OA] is the sliding abrasion (mechanical damage) and the (C+S) [OA] is the corrosion related component in the outer area.

Total mass loss with cathodic protection (CP)

The total mass losses with cathodic protection of the steels were measured directly from the experiments (see Figure 3). The application of CP resulted in reductions in the overall material mass loss of both materials. It is clear that the mass loss on the UNS G10400, when the cathodic current was applied, was decreased from 11.7 mg to 6.5 mg (68 %), whereas the UNS S31600 mass loss dropped by 18 %. This signifies that the corrosion related component (C+S) is playing a more substantial role on the material degradation of the medium carbon steel and it has far less influence on the stainless steel. Thus, the important factor is likely to be that the solid particles break down the surface protective film of the stainless steel but the reformation rate is high.

Since the application of cathodic protection supresses any corrosion reaction, the total mass loss represents the erosion damage inside the wear scar and the sliding abrasion which takes place outside the wear scar (Equation 4)

$$TML\ (CP) = E\ [DIZ] + SA\ [OA] \qquad \text{Equation 4}$$

Erosion damage on the direct impinged zone (DIZ)

The mechanical damage that occurred in the direct impinged zone (DIZ) was measured through the volume loss calculations on the cathodically protected tested coupons. Table 4 illustrates the mass loss due to the mechanical damage on the wear scar.

Materials	Volume (mm^3)	Density (kg/cm^3)	Mass (mg)
UNS S31600 (CP) [DIZ]	0.40	8.00	3.2
UNS G10400 (CP) [DIZ]	0.49	7.85	3.9

Table 4. Mass loss calculated from the volumetric analysis of the wear scar for cathodically protected specimens.

The UNS G10400 steel exhibited significantly higher erosion deterioration than UNS S31600. Taking into account the similar hardness of the two steels (Table 1), this is evidence of the relative insensitivity of erosion to target hardness. Although it is generally accepted that material hardness is an important parameter in terms of damage by abrasive wear, for other types of wear (e.g. erosion), however, such a simple linkage, with hardness alone, is less appropriate. The elastic modulus is considered to be another important property with a high value of the ratio of hardness to elastic modulus being desirable [22]. It any case, for a high velocity impinging jet attempted correlations with conventional mechanical properties may be less relevant than the incorporation of mechanical properties determined under high-strain-conditions.

Corrosion and synergy on the direct impinged zone (DIZ)

According to Figure 8, the volumetric losses, in the wear scars on both materials with and without the application of CP were similar. This means that, in the material/testing conditions of this study, the material loss on the direct impinged region is purely by mechanical action and the corrosion related component is negligible on the direct impinged zone. The properties of the erodent should

have played some role on this erosion domination. This erosion domination is likely to have been associated with the erodent properties (size/shape) and the jet velocities.

Sliding abrasion on the outer area (OA)

Through evaluation of Equation 4, the mechanical sliding abrasion damage was determined for both materials and the data is obtained as follows:

SA [OA] = TML (CP) - E [DIZ]

Medium Carbon steel: SA [OA] = 6.5 – 3.9 = 2.6mg
Stainless steel: SA [OA] = 4.8 – 3.2 = 1.6mg

This difference between the two materials is rather surprising, given that it is generally considered that damage by abrasion is related to target material hardness [22].

Corrosion and synergy on the outer area (OA)

The contribution of corrosion and synergy on the outermost area was defined by the subtraction of the sliding abrasion damage from the calculated overall mass loss on the outer area, as shown below:

(C+S) [OA] = ML [OA] – SA [OA]

Medium Carbon steel: (C+S) [OA] = 7.8 – 2.6 = 5.2mg
Stainless steel: (C+S) [OA] = 2.7 – 1.6 = 1.1mg

On the outer area (OA), the stainless steel exhibited good performance as the corrosion related component was substantially lower than that of carbon steel. The stainless steel suffered less corrosion, apparently, because of the passive film, which wasn't breaking down as much as in the direct impinged zone because the flow velocity and sand concentration was lower in the outer area. On the other hand, the carbon steel was not protected by any protective film which resulted in a greater mass loss due to corrosion related phenomena on the outer area.

The quantitative material losses, shown in Figure 9, demonstrate the substantial benefits of the expanded assessment of erosion-corrosion testing that forms the basis of this paper.

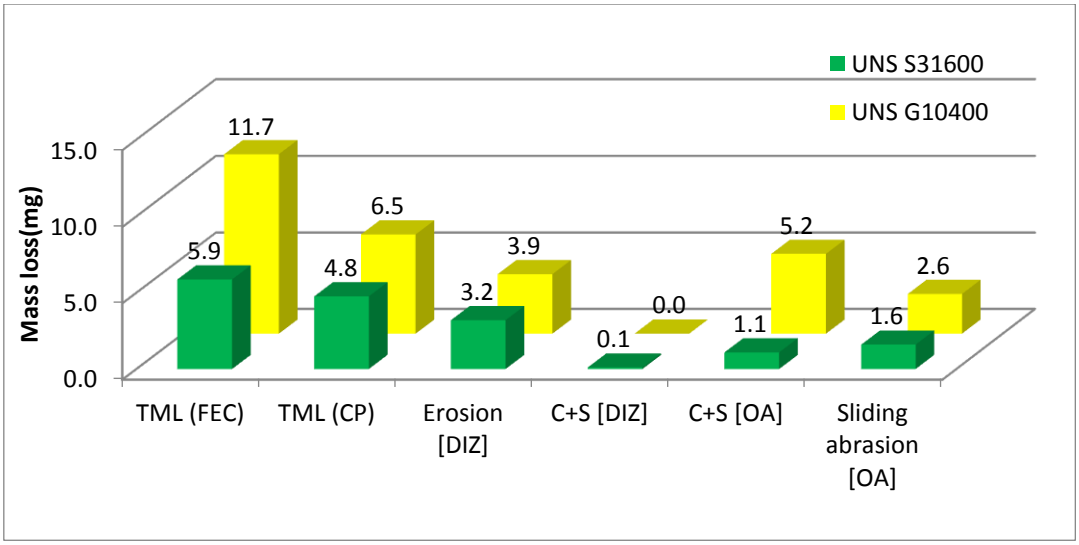

Figure 9. Discrimination of the different material degradation processes on the UNS S31600 and UNS G10400 steels.

The findings have facilitated quantification of the effect of the extreme angles of impingement, i.e. 90° and 0° from one jet impingement test and also, isolation of the mass losses taking place on the direct impinged zone and the outer area. They have also demonstrated the differentiation between the mechanical deterioration mechanisms of erosion and sliding abrasion and shown that sliding abrasion contributes significantly to the mechanical damage resulting from the action of an impinging jet on the large component.

In general, this procedure enables a wider appreciation to be obtained of the comparative performances, of different materials/coatings under solid liquid impingement, than is acquired by simply comparing measured mass losses.

5. Conclusions

An extended evaluation procedure has been presented that:

1. Contributes to the understanding of the fundamental mechanisms of corrosive wear on a component subjected to a locally-impinging, solid/liquid stream.
2. Enhances the assessment of the performance of different materials or surface engineering treatments in various corrosive wear environments.

In the present study, this methodology has been used to compare the behaviour of the UNS S31600 and UNS G10400 and the findings can be summarized as follows:

1. The superior performance of stainless steel (UNS S31600) in comparison with carbon steel (UNS G10400) has been shown to involve benefits in respect of pure mechanical damage (in the wear scar and outer area) and also in terms of corrosion related phenomena.
2. UNS S31600 has been shown to exhibit greater erosion-corrosion performance at both angles of impingement (90° and also at the glancing angle of 0°).
3. The application of cathodic protection was effective, since it decreased the mass loss of the steels substantially. However, the wear scar volumes were similar in free erosion corrosion conditions and with cathodic protection. This displays the erosion dominated degradation processes occurring inside the wear scar under the conditions of this study.

4. The experimental results have illustrated that there are some limitations in simple correlation of corrosive wear damage with target hardness.

Acknowledgement

The authors would like to acknowledge the support for this study, which was provided by the Weir Group PLC via its establishment of the Weir Advanced Research Centre (WARC) at the University of Strathclyde.

6. References

[1] M. Reyes, A. Neville, Mechanisms of erosion-corrosion on a cobalt-base alloy and stainless-steel UNS S17400 in aggressive slurries, J. Mater. Eng. Perform. 10 (2001) 723–730.

[2] A. Neville, X. Hu, Mechanical and electrochemical interactions during liquid – solid impingement on high-alloy stainless steels, Wear. 251 (2001) 1284–1294.

[3] R.J.K. Wood, J.C. Walker, T.J. Harvey, S. Wang, S.S. Rajahram, Influence of microstructure on the erosion and erosion–corrosion characteristics of 316 stainless steel, Wear. 306 (2013) 254–262.

[4] H.M. Clark, H.. Hawthorne, Y. Xie, Wear rates and specific energies of some ceramic, cermet and metallic coatings determined in the Coriolis erosion tester, Wear. 233-235 (1999) 319–327.

[5] H.H. Tian, G.R. Addie, E.P. Barsh, A new impact erosion testing setup through Coriolis approach, Wear. 263 (2007) 289–294.

[6] R.J.K. Wood, Erosion–corrosion interactions and their effect on marine and offshore materials, Wear. 261 (2006) 1012–1023.

[7] M.M. Stack, G.H. Abdulrahman, Mapping erosion–corrosion of carbon steel in oil–water solutions: Effects of velocity and applied potential, Wear. 274-275 (2012) 401–413.

[8] C.G. Telfer, M.M. Stack, B.D. Jana, Particle concentration and size effects on the erosion-corrosion of pure metals in aqueous slurries, Tribol. Int. 53 (2012) 35–44.

[9] M. Parsi, K. Najmi, F. Najafifard, S. Hassani, B.S. McLaury, S.A. Shirazi, A comprehensive review of solid particle erosion modeling for oil and gas wells and pipelines applications, J. Nat. Gas Sci. Eng. 21 (2014) 850–873.

[10] J. Postlehwaite, S. Nesic, G. Adamopoulos, D.J. Bergstrom, Predictive models for erosion-corrosion under disturbed flow conditions, Corros. Sci. 35 (1993) 627–633.

[11] A. Gnanavelu, N. Kapur, A. Neville, J.F. Flores, An integrated methodology for predicting material wear rates due to erosion, Wear. 267 (2009) 1935–1944.

[12] C.I. Walker, P. Robbie, Comparison of some laboratory wear tests and field wear in slurry pumps, Wear. 302 (2013) 1026–1034.

[13] M. Divakar, V.K. Agarwal, S.N. Singh, Effect of the material surface hardness on the erosion of AISI316, Wear. 259 (2005) 110–117.

[14] M.A. Islam, Z.N. Farhat, Effect of impact angle and velocity on erosion of API X42 pipeline steel under high abrasive feed rate, Wear. 311 (2014) 180–190.

[15] Q.B. Nguyen, V.B. Nguyen, C.Y.. Lim, Q.T. Trinh, S. Sankaranarayanan, Y.W. Zhang, et al., Effect of impact angle and testing time on erosion of stainless steel at higher velocities, Wear. 321 (2014) 87–93.

[16] I. Finnie, Some reflections on the past and future of erosion, Wear. 186-187 (1995) 1–10.

[17] J.M. Perry, T. Hodgkiess, A. Neville, Some aspects of the erosion and corrosion behaviour of a WC-Co-Cr HVOF sprayed coating, Proc. Int. Therm. Spray Conf. ASM ITSC. (2000).

[18] N. Andrews, L. Giourntas, A.M. Galloway, A. Pearson, Effect of impact angle on the slurry erosion-corrosion of Stellite 6 and SS316, Wear. 320 (2014) 143–151.

[19] D. Matzavinos, Durability studies relevant to marine equipment, University of Glasgow, 2001.

[20] J.I. Ukpai, R. Barker, X. Hu, A. Neville, Exploring the erosive wear of X65 carbon steel by acoustic emission method, Wear. 301 (2013) 370–382.

[21] R.J. Barker, Erosion-Corrosion of Carbon Steel Pipework on an Offshore Oil and Gas Facility, University of Leeds, 2012.

[22] A. Matthews, A. Leyland, Materials related aspects of nanostructured tribological coatings, 51st SVC TechCon. (2008).